Programmable RF-to-optical frequency synthesis with fully stabilized dual-microcomb

Saleha Fatema[1†], Kaiyi Wu[1,2*†], Nathan P. O'Malley[1], Cong Wang[1,3], Marcello Girardi[2], Mohammed S. Alshaykh[4], Andrew M. Weiner[1], Victor Torres-Company[2] and Jason D. McKinney[1*]

[1]School of Electrical and Computer Engineering, Purdue University, West Lafayette, 47907, IN, USA.
[2]Department of Microtechnology and Nanoscience, Chalmers University of Technology, SE-41296, Sweden.
[3]Currently with Department of Surgery, University of Pittsburgh, 15219, PA, USA.
[4]Electrical Engineering Department, King Saud University, Riyadh, 11421, Saudi Arabia.

*Corresponding author(s). E-mail(s): wu1871@purdue.edu; mckinnjd@purdue.edu;
†These authors contributed equally to this work.

1 RF-to-optical frequency synthesis

As described in the main text, four heterodyne beats from the dual-microcomb are detected. The repetition rate difference δf_{rep} is detected at both sides of the pump:

$$\delta f_{\mathrm{rep}+} = \delta f_{\mathrm{rep}-} = f_{\mathrm{rep},1} - f_{\mathrm{rep},2}. \tag{S1}$$

The Vernier beat f_{Vernier} is detected at the Vernier overlap point of the two sets of comb lines at 2 μm wavelength:

$$f_{\mathrm{Vernier}} = N f_{\mathrm{rep},1} - (N+1) f_{\mathrm{rep},2}, \tag{S2}$$

where N is the mode number relative to the pump. In this work, we have utilized both $N = 44$ and $N = 45$. The modified f-2f beat $f_{\mathrm{f-2f}}$ is obtained by SFG between a main comb line $f_{\mathrm{ceo},1} + 166 f_{\mathrm{rep},1}$ and a Vernier comb line

$f_{\mathrm{ceo},2} + 179 f_{\mathrm{rep},2}$ at 2 μm wavelength and subsequent beating of this line with a main comb line (the short wavelength dispersive wave) $f_{\mathrm{ceo},1} + 342 f_{\mathrm{rep},1}$, such that:

$$f_{\mathrm{f-2f}} = f_{\mathrm{ceo},2} + 179 f_{\mathrm{rep},2} - 176 f_{\mathrm{rep},1}. \tag{S3}$$

The noise-suppressed repetition rates for both combs that are derived from Eqs. S1 & S2, whose generation method is described in Methods, can be expressed as:

$$\frac{f_{\mathrm{rep},1}}{N+1} = \frac{\delta f_{\mathrm{rep}-}}{2} + \frac{\delta f_{\mathrm{rep}+}}{2} - \frac{f_{\mathrm{Vernier}}}{N+1}, \tag{S4}$$

$$\frac{f_{\mathrm{rep},2}}{N} = \frac{\delta f_{\mathrm{rep}-}}{2} + \frac{\delta f_{\mathrm{rep}+}}{2} - \frac{f_{\mathrm{Vernier}}}{N}. \tag{S5}$$

Together with the shared pump condition:

$$f_{\mathrm{pump}} = f_{\mathrm{ceo},1} + 216 f_{\mathrm{rep},1} = f_{\mathrm{ceo},2} + 220 f_{\mathrm{rep},2}, \tag{S6}$$

we can derive the expressions of the optical frequencies for both combs using the equations listed above.

In the first scenario, we lock the $f_{\mathrm{rep},1}/4(N+1)$, f_{Vernier} and $f_{\mathrm{f-2f}}$ beats. The frequencies of the comb lines can be expressed in terms of these beats. For the main comb, as we showed in the main text:

$$\begin{aligned} f_{\mathrm{m},1} &= m_1 f_{\mathrm{rep},1} + f_{\mathrm{ceo},1} \\ &= (m_1 - 40 + \frac{41N}{N+1}) f_{\mathrm{rep},1} - \frac{41}{N+1} f_{\mathrm{Vernier}} + f_{\mathrm{f-2f}}. \end{aligned} \tag{S7}$$

We can also write the expression for the Vernier comb lines $f_{\mathrm{m},2}$:

$$\begin{aligned} f_{\mathrm{m},2} &= m_2 f_{\mathrm{rep},2} + f_{\mathrm{ceo},2} \\ &= [(m_2 - 179)\frac{N}{N+1} + 176] f_{\mathrm{rep},1} - \frac{m_2 - 179}{N+1} f_{\mathrm{Vernier}} + f_{\mathrm{f-2f}}. \end{aligned} \tag{S8}$$

In the experiment, we adopt $N = 45$ in this scenario. At the pump frequency, we have $m_1 = 216$ and $m_2 = 220$. With the knowledge that $f_{\mathrm{rep},1} \approx 896$ GHz, $f_{\mathrm{Vernier}} \approx 11$ GHz and $f_{\mathrm{f-2f}} \approx 12$ GHz, the first term in Eqs. S7 & S8 is four orders of magnitude larger than the other two terms. Hence, the stability of the repetition rate lock dominates the stability of the optical frequencies.

In the second scenario, we lock $f_{\mathrm{rep},2}/4N$, f_{Vernier} and $f_{\mathrm{f-2f}}$ beats. We can also write the comb line frequencies in terms of these three beats. For the main comb, we have:

$$\begin{aligned} f_{\mathrm{m},1} &= m_1 f_{\mathrm{rep},1} + f_{\mathrm{ceo},1} \\ &= [(m_1 - 40)\frac{N+1}{N} + 41] f_{\mathrm{rep},2} + \frac{m_1 - 40}{N} f_{\mathrm{Vernier}} + f_{\mathrm{f-2f}}. \end{aligned} \tag{S9}$$

And for the Vernier comb, we have:

$$\begin{aligned} f_{\mathrm{m},2} &= m_2 f_{\mathrm{rep},2} + f_{\mathrm{ceo},2} \\ &= (m_2 - 179 + 176\frac{N+1}{N}) f_{\mathrm{rep},2} + \frac{176}{N} f_{\mathrm{Vernier}} + f_{\mathrm{f-2f}}. \end{aligned} \tag{S10}$$

In this case, we adopt $N = 44$, and $f_{\mathrm{rep},2} \approx 876$ GHz, $f_{\mathrm{Vernier}} \approx -9$ GHz and $f_{\mathrm{f-2f}} \approx 12$ GHz. Similar to the first scenario, the repetition rate lock is still dominant, but the contribution from the f_{Vernier} lock is a few times higher in this case.

2 Stability without and with noise-suppression

Repetition rate detection using the Vernier approach can be directly obtained through the electronic division and mixing of f_{Vernier} and one of the δf_{rep}, as described in Ref. [1] (also illustrated in Fig. S1a). Initially, we locked $f_{\mathrm{rep},1}$ derived from this method, along with the locking of f_{Vernier} and $f_{\mathrm{f-2f}}$, to fully stabilize the dual-comb. The fractional Allan deviation of the pump, shown in Fig. S1b, reveals that at short gate times, the Allan deviation follows $1/\tau$, indicating successful phase-locking of the pump frequency to the reference. However, at longer gate times (approximately 1 s), the Allan deviation reaches a plateau- a behavior previously observed in other studies [2, 3]. Since the pump frequency is primarily determined by the repetition rate of the comb,

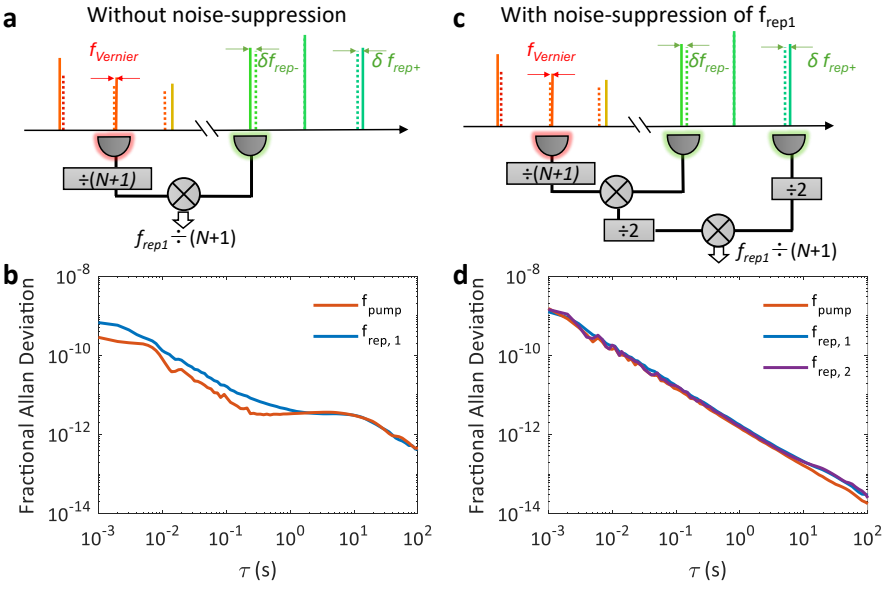

Fig. S1 Stability of optical lines and repetition rates without and with noise suppression. Simplified schematic of the experimental setup and fractional Allan deviation measurements of f_{pump}, $f_{\mathrm{rep},1}$, and $f_{\mathrm{rep},2}$ when (**a, b**) $f_{\mathrm{rep},1}$ is extracted without noise suppression, (**c, d**) $f_{\mathrm{rep},1}$ is extracted with noise suppression,

we employed a separate out-of-loop verification method using an electro-optic comb. We found that the stability of the out-of-loop repetition rate closely mirrors that of the pump. Based on our earlier research utilizing the Vernier scheme for optical frequency division, we attribute this plateau to interferometric phase fluctuations in dual-comb systems. This issue can be addressed using a differential noise suppression scheme [3]. In this technique, the differential mode noise of the two δf_{rep} signals is canceled by summing the δf_{rep} beats detected from both sides of the pump. To avoid second-order harmonics from overlapping at the same frequency, one of the δf_{rep} signals is slightly shifted by an RF signal using an RF frequency mixer.

This work simplifies the scheme by changing the mixing and division order. The offset between the two δf_{rep} beats during the electronic summation is achieved using f_{Vernier} for frequency shifting. This results in the divided, noise-suppressed repetition rate, as illustrated in Fig. S1c, and eliminates the need for an additional RF source. The division factors are adjusted to extract only one f_{rep} at a time. The out-of-loop verification of $f_{\mathrm{rep},1}$ is represented by the blue line in Fig. S1d, which shows that the $f_{\mathrm{rep},1}$ is being stabilized without the effect of interferometer noise. To achieve complete dual-comb stabilization, we also stabilize the other two beats (f_{Vernier} and $f_{\mathrm{f-2f}}$), and perform out-of-loop verification of the other repetition rate ($f_{\mathrm{rep},2}$) and the pump. As shown in Fig. S1d, the results confirm that interferometric noise in our dual-comb system is effectively suppressed.

Additionally, we plot the fractional Allan deviation of seven optical comb lines shown in the main text (Fig. 2c) in Fig. S2, and observe that the Allan deviation matches and closely follows the stability of the f_{rep}s. This demonstrates that the stability of the optical comb lines reaches down to that of two repetition rates. Importantly, the locking scheme works equally well regardless of which repetition rate is noise-suppressed and being locked. In the main

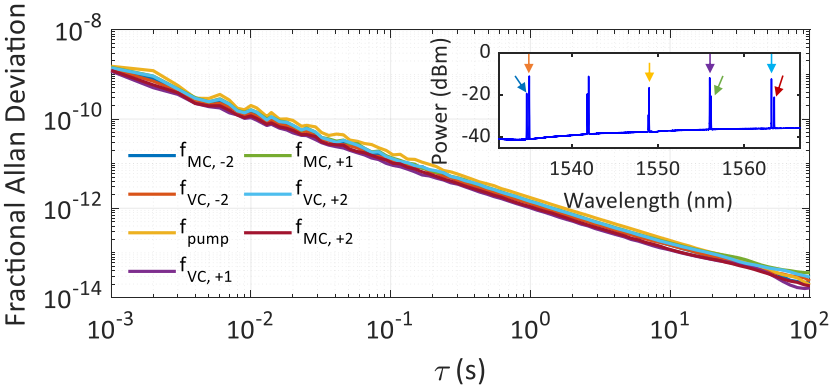

Fig. S2 Stability of optical lines. Fractional Allan deviation of seven comb lines from the main and Vernier combs. The inset plot shows the optical spectrum of the comb lines, and the color of the arrows pointing to the comb lines corresponds to those lines in the figure legend.

text, we have also extracted and stabilized the noise-suppressed $f_{\mathrm{rep},2}$ with $N = 44$ instead of $f_{\mathrm{rep},1}$, and found a similar Allan deviation (Fig.2b).

3 Demonstration of reconfigurable EO comb

To fill the $\sim$ 1 THz gap, we use an EO comb generator consisting of an IM followed by several phase modulators (PMs) [4] with $\sim$ 10 GHz spaced comb lines. As illustrated in Fig. 4a, the two frequency-divided repetition rates $f_{\mathrm{rep},1}/2(N+1)$ and $f_{\mathrm{rep},2}/2N$ derived from the dual-comb system serve as the RF drives for the EO comb generators for the main and Vernier combs, respectively. By controlling the division factors (multiples of $(N+1)$ and N for the main and Vernier comb, respectively), we can reconfigure the optical grids using simple RF electronic frequency dividers. To demonstrate the reconfigurability, we select three lines from each microcomb on the blue side of the pump (slightly different from the three lines used in the main text). Figure S3a shows an example of the optical spectrum with three lines from the Vernier comb, after being optically amplified by an erbium-doped fiber amplifier (EDFA). Note that the number of comb lines that can be employed is mainly limited by the gain bandwidth of our EDFA. Figure S3b shows the optical spectrum of the EO comb lines filling the gaps between the microcomb lines of Fig. S3a with $\sim$10 GHz driving frequency. Further reduction in the line spacing is achieved by further dividing the RF drive and using additional modulators. For example, in Fig. S3c, we introduce a PM driven by the $\sim$ 10

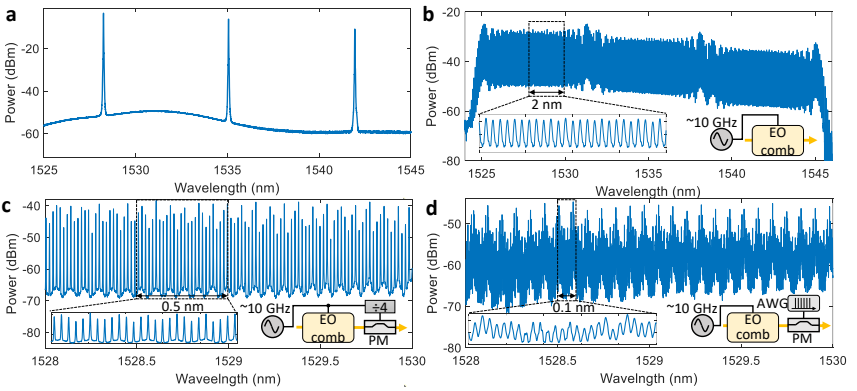

Fig. S3 Reconfigurability of the THz frequency division. (**a**) The optical spectrum of three Vernier comb lines, selected by a programmable optical filter and amplified by an EDFA. (**b**) Optical spectrum of the EO comb with $\sim$ 10 GHz line spacing. The inset shows the zoom-in spectrum within 2 nm span. (**c**) Optical spectrum of the comb with $\sim$ 2.5 GHz line spacing generated by an EO comb driven at $\sim$ 10 GHz, followed by a PM driven at $\sim$ 2.5 GHz. The inset shows the zoomed-in spectrum within a 0.5 nm span. (**d**) Optical spectrum of the comb with $\sim$ 500 MHz line spacing generated by an EO comb driven at $\sim$ 10 GHz, followed by a PM driven by a multi-tone from 500 MHz to 5 GHz. The inset shows the zoomed-in spectrum within a 0.1 nm span. The schematic on the lower right corner of (b-d) illustrates the setup for generating the spectrum with optical input from (a).

GHz signal with an additional division factor of 4, which reduces the line spacing to ~ 2.5 GHz. This PM can also be driven by multitone or chirp signals [5] to further reduce the spacing to ~ 500 MHz, as shown in Fig. S3d. However, in this case, the driving signal is generated using an external arbitrary waveform generator (AWG) that is synchronized to the common RF clock reference used for dual-comb stabilization, and the signal must be adjusted to match the microcomb repetition rate. We note that in the latter case, the driving frequency no longer automatically tracks the microcomb repetition rates, as such a complex driving signal is manually defined.

4 Frequency calibration of additional lasers

In addition to calibrating the NewFocus laser discussed in the main text, we calibrate two other lasers to demonstrate the versatility of our approach. The experimental setup is similar to that presented in the main text, with the lasers being an Agilent (81680A) Fabry-Pérot (FP) laser and a Koheras (Adjustik KOH1755) fiber laser. We first assess the frequency precision of our stabilized dual-comb system by measuring the stability of the pump by beating it with a comb line from a stable fiber comb using a frequency counter with a 100-ms gate time. The top panel of Fig. S4a shows the trace of the pump frequency fluctuation Δf_{pump} with a standard deviation of 1.2 kHz (top panel of Fig. S4b). This indicates that our system can provide kHz-level

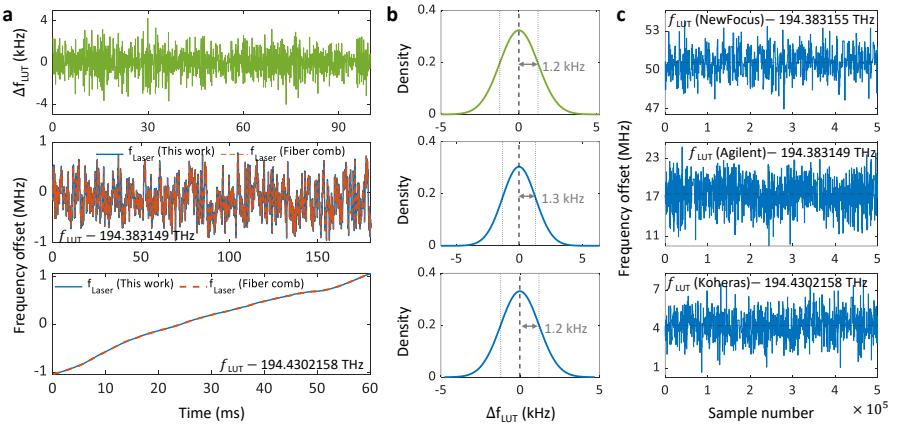

Fig. S4 Frequency precision measurement along with calibration of two additional lasers. (**a**) Top panel- Frequency fluctuation of the pump when the dual-comb system is fully stabilized. Middle and bottom panel- The calibrated wavelength of LUT measured by our dual-comb method and a stable fiber comb for the Agilent laser (middle) and the Koheras fiber laser (bottom). (**b**) Probability density function of the pump fluctuation (top) and frequency difference between our dual-comb method and the stable fiber comb for the Agilent laser (middle) and the Koheras fiber laser (bottom). The dashed lines indicate the mean, and the dotted lines indicate the standard deviation between the two measurement methods. (**c**) Wavemeter data measured for the NewFocus laser (top), the Agilent laser (middle), and the Koheras fiber laser (bottom). Dashed horizontal lines in each plot indicate the mean difference.

frequency precision at a 100 ms gate time, with the capability of achieving better resolution at longer gate times.

The middle and the bottom panel of Fig. S4a shows the laser frequencies measured using the Vernier dual-comb approach (blue lines), alongside the frequencies measured using a wavemeter and a commercial fiber comb (orange dashed lines) for the Agilent and Koheras lasers, respectively. The Agilent laser (middle panel) exhibits more frequency fluctuations but less drift over time, while the Koheras laser (bottom panel) shows less frequency fluctuation but noticeable drift in the time trace. This is because the Agilent FP laser has a larger linewidth and good wavelength locking, whereas the fiber laser has a much narrower linewidth but is experiencing thermal drift. The middle and the bottom panel of Fig. S4b shows the probability density plot of frequency differences between the laser frequencies measured using our dual-comb system and the commercial fiber comb. The standard deviations of the differences for the Agilent and Koheras lasers are 1.3 kHz and 1.2 kHz, respectively, matching closely with the frequency precision of our dual-comb system shown in the top panel of Fig. S4b.

We also monitored the wavemeter data used to resolve the mode number for the fiber frequency comb (Fig. S4c). The commercial wavemeter cannot resolve the MHz-level wavelength fluctuation for all LUTs, appearing as a straight line for the recorded wavelength. We also observe a frequency offset of ∼17 MHz for the Agilent laser (middle plot) and ∼4 MHz for the Koheras laser (bottom plot) from the frequencies measured using our approach (and the commercial fiber approach). The wavemeter data from the NewFocus laser is also plotted on the top panel of Fig. S4c, which shows a difference of ∼50 MHz. This suggests that our dual-comb system can serve as an optical wavemeter with much higher resolution.

5 Frequency calibration of dynamic LUT with longer measurement time

In the main text, we used two EO combs driven at a ∼ 10 GHz drive for dynamic laser frequency tracking and were limited to a 5-ms-long data because of the memory of the DSA used. This can be addressed using an electronic frequency divider, which reduces the maximum beat frequency at the cost of a few gigahertz of unresolved frequency within one FSR, as well as a reduction in the maximum resolvable chirp rate [6]. To circumvent this limitation and permit longer recordings, we further reduce the resolution of the Vernier comb by adding a PM after the EO comb, which is driven by multitone RF signal (spanning from 500 MHz to 5 GHz with a 500 MHz step) generated from an AWG (synchronized to the common 10-MHz clock), as shown in Fig. S3d. We can thus reduce the sampling rate of the DSA to 500 MHz in order to capture RF signals within 250 MHz. Portions of the recorded spectrograms are shown in Fig. S5a. The main combline spacing remains the same as before (10 GHz) and therefore, the beat note is captured only when the laser is <250 MHz away

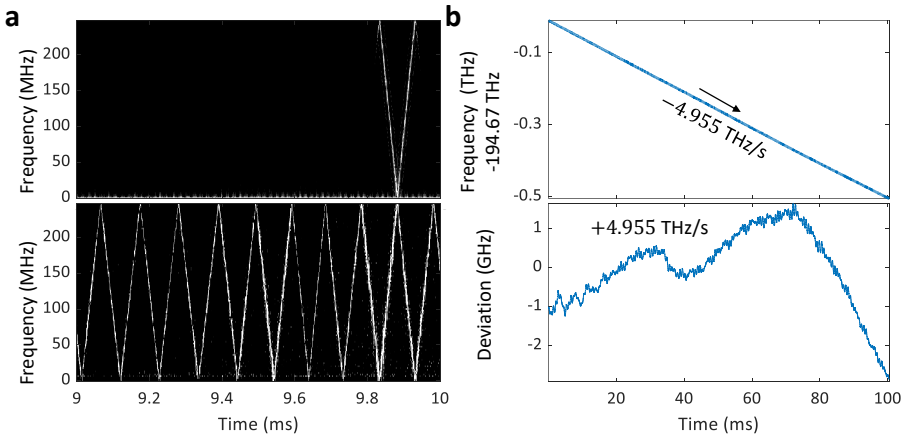

Fig. S5 Frequency calibration of a sweeping laser. (**a**) A portion of the spectrograms of the heterodyne signals between the sweeping laser and the main comb at ∼10 GHz line spacing (upper) and the Vernier comb at ∼500 MHz line spacing, respectively. (**b**) Upper: the calibrated wavelengths of the laser calculated from the Vernier comb beats. Lower: wavelength deviation from the linear sweeping speed.

from the comb lines (Fig. S5a top). We calibrate the absolute laser frequencies when the beat notes on both spectrograms are recorded, and we keep track of the sweeping frequencies calculated from the spectrogram of the Vernier comb. Figure S5b shows the calibrated laser frequencies (top) sweeping at $-\sim$4.955 THz/s ($\sim$39.30 nm/s) with an increased recording time of 100 ms, as well as the nonlinearity of the wavelength sweep (bottom).

6 Unambiguous laser frequency calibration using a dual-comb scheme

Utilizing the dual-comb approach (restricted to one side of the pump), it is possible to achieve an unambiguous CW laser frequency measurement, whether it lies on the blue or red side of the pump. This section provides further details on the frequency calibration process. In this experiment, we use comb lines on the blue side of the pump. When a continuous wave laser beats with the dual-comb, each comb produces two beat signals through beating with the n^{th} and $(n+1)^{th}$ lines, i.e. Δf_{n1} and $f_{\mathrm{rep},1}/90 - \Delta f_{\mathrm{n1}}$ for the main comb, and Δf_{n2} and $f_{\mathrm{rep},2}/88 - \Delta f_{\mathrm{n2}}$ for the Vernier comb. Since both beat signals from the same comb carry identical information, only the smaller frequency components, $\leq f_{\mathrm{rep},1}/90/2, \leq f_{\mathrm{rep},2}/88/2$, are recorded. We denote the measured beats as δf_1 for the main comb and δf_2 for Vernier comb, which can be beating with either the n^{th} or $(n+1)^{th}$ lines.

We can easily identify which lines the measured beats are beating with for both combs from their relative values, since we know $f_{\mathrm{rep},2}/88 - f_{\mathrm{rep},1}/90 = \Delta f_{\mathrm{r}} > 0$. Figure S6 illustrates the different cases when δf_1 and δf_2 are

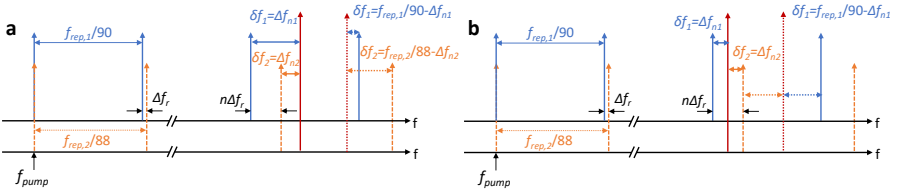

Fig. S6 Laser frequency calibration in dual-comb scheme. (**a**) The difference of the two detected beats is a constant, which is an integral multiple of Δf_{r}, as a result of LUT beats with either the n^{th} (solid line) or $(n+1)^{th}$ (dotted line) lines. (**b**) The summation of the two detected beats is a constant, which is either an integral multiple of Δf_{r} (solid line) or $f_{\mathrm{rep},1}/90 - n\Delta f_{\mathrm{r}}$ (dotted line).

detected. If the difference of δf_1 and δf_2 remains constant which is an integral multiple of Δf_{r}, as illustrated in Fig. S6a , we have either $\delta f_1 > \delta f_2$ for $\delta f_1 = \Delta f_{\mathrm{n1}}$ and $\delta f_2 = \Delta f_{\mathrm{n2}}$, or $\delta f_1 < \delta f_2$ for $\delta f_1 = f_{\mathrm{rep},1}/90 - \Delta f_{\mathrm{n1}}$ and $\delta f_2 = f_{\mathrm{rep},2}/88 - \Delta f_{\mathrm{n2}}$. If the summation of δf_1 and δf_2 remains constant, as illustrated in Fig. S6b, we can evaluate whether this sum is an integral multiple of Δf_{r} to differentiate the two cases illustrated by the solid and dotted lines for LUT in Fig. S6b. We have either $\delta f_1 + \delta f_2 = n\Delta f_{\mathrm{r}}$ for $\delta f_1 = \Delta f_{\mathrm{n1}}$ and $\delta f_2 = \Delta f_{\mathrm{n2}}$, or $\delta f_1 + \delta f_2 = f_{\mathrm{rep},1}/90 - n\Delta f_{\mathrm{r}}$ for $\delta f_1 = f_{\mathrm{rep},1}/90 - \Delta f_{\mathrm{n1}}$ and $\delta f_2 = \Delta f_{\mathrm{n2}}$.

References

[1] Wu, K. *et al.* Vernier microcombs for high-frequency carrier envelope offset and repetition rate detection. *Optica* **10** (5), 626–633 (2023) .

[2] Drake, T. E. *et al.* Terahertz-rate kerr-microresonator optical clockwork. *Physical Review X* **9** (3), 031023 (2019) .

[3] Wu, K. *et al.* Vernier microcombs for integrated optical atomic clocks. *Nature Photonics* 1–7 (2025) .

[4] Metcalf, A. J., Torres-Company, V., Leaird, D. E. & Weiner, A. M. High-power broadly tunable electrooptic frequency comb generator. *IEEE Journal of Selected Topics in Quantum Electronics* **19** (6), 231–236 (2013) .

[5] Long, D. A., Fleisher, A. J., Plusquellic, D. F. & Hodges, J. T. Multiplexed sub-doppler spectroscopy with an optical frequency comb. *Physical Review A* **94** (6), 061801 (2016) .

[6] Yang, Q.-F. *et al.* Vernier spectrometer using counterpropagating soliton microcombs. *Science* **363** (6430), 965–968 (2019) .